Intersubband gain without global inversion through dilute nitride band engineering

PEREIRA, Mauro <http://orcid.org/0000-0002-2276-2095> and TOMIĆ, Stanko

Citation:

Copyright and re-use policy

Intersubband gain without global inversion through dilute nitride band engineering

Mauro F. Pereira Jr[*]

Materials and Engineering Research Institute,

Sheffield Hallam University, Howard Street, Sheffield, S1 1WB, UK

Stanko Tomić[†]

Computational Science and Engineering Department,

STFC Daresbury Laboratory, Cheshire WA4 4AD, UK

(Dated: January 14, 2011)

Abstract

We investigate the possibility of inter-conduction band without global inversion by engineering the conduction band effective masses so that the upper lasing subband has an effective mass considerably smaller than the lower lasing subband that could not be obtained in conventional III-V materials. We recover the expected dispersive gain shape for similar masses and contrasting results if the effective masses characterizing the relevant subbands are very different.

PACS numbers: 42.55.Px,78.66.-w,71.20.Nr,78.67.De

[*]Electronic address: M.Pereira@shu.ac.uk

[†]Electronic address: stanko.tomic@stfc.ac.uk

Intersubband (ISB) devices like the quantum cascade laser (QCL), in which the frequecy of the emitted radiation is not limited by the semiconductor bandgap, can unleash the potential for many applications in the far infrared [1]. Mid infrared (MIR) QCLs already deliver high power at room temperature [2] but at present the maximum operating temperature of a THz device is 186 K emitting at 3.9 THz [3]. Conventional designs emitting at a given frequency $\hbar\omega$ seem to have a maximum operating temperature $T_{\max} \approx \hbar\omega/k_B$ [4]. The main difficulty at high temperatures is achieving population inversion and ISB lasing without inversion (LWI) [5–7], may be a solution for this microscopic bottleneck. ISB LWI has been realised experimentally by exploiting the nonparabolicity of the conduction subbands and local population inversion near $\mathbf{k} = 0$ even though the lowest subband may have larger global occupation [5]. Later on, valence-band-based designs have been proposed [8] and more recently a mechanism combining band nonparabolicity with a k-space filtering in the TE mode of hole intervalence transitions in quantum wells has been introduced [9]. However, holes thermalise very fast and it would be ideal to be able to exploit extreme nonparabolicity in the conduction bands. This can be achieved, e.g. in dilute nitride quantum wells [10–12]. ISB transitions in a similar dilute nitride system (InGaNAs-based) have been investigated both theoretically [13, 14] and experimentally [15]. Previous simulations indicate a potential for both telecom Ref. 13 and MIR transitions in the (4 μm) ranges [14]. Models such in Ref. [13] use phenomenological Lorentzian broadenings and can be used to fit experimental absorption but should not be applied for gain calculations. Among other limitations, they lead to strong unphysical absorption features below the gain. They further do not include relevant scattering mechanisms and many particle corrections that increase their relevances as the electronic density increases to reach the gain regime [16].

In this paper we investigate the possibility of ISB gain without global inversion by engineering the conduction band effective masses using the Nonequilibrium Green's Functions (NGF) approach. The upper gain subband has an effective mass made considerably smaller than the lower lasing subband that could not be obtained in conventional III-V materials where the electron effective mass is proportional to energy gap. In this proof of concept we take a simple system - a single quantum well which nevertheless delivers gain at a relevant MIR wavelength (around 2 μm). The strong interaction between the N resonant states and the conduction band edge means that the conventional 8-band $\mathbf{k}\cdot\mathbf{p}$ method cannot be applied directly to GaAsN and related heterostructures. One must include the interaction

between the N resonant states and the conduction band edge to describe the variation of the (zone-centre) conduction band edge energy with N. This leads to a modified ten-band Hamiltonian as shown in Ref. 17. The ten-band Hamiltonian describes on average interaction of the all N atoms with the host material. It has been observed that when N-related cluster states lie in close proximity, on energy scale, to the conduction band edge of the host material, the electron effective mass have even stronger increase with nitrogen concentration [18, 19]. This was explained by hybridisation of the N-cluster states to Γ character of the host material conduction band. [20] Consequently we have modified the 10-band $\mathbf{k}\cdot\mathbf{p}$ Hamiltonian to describe the average interaction of the N, NN-pairs and other N-cluster states with the host material. To achieve this the resonant N level (that on average describes all N related states) is set at $E_N = 1.35$ eV. Coupling between those states and the Γ band edge (1.42 eV) of the host GaAs material is determined by the relations $V_{Nc} = 2.45\sqrt{x}$ where x is the nitrogen concentration. Other Hamiltonian matrix elements related to the GaAs host material are taken from standard literature [21]. The absorption $\alpha(\omega)$ or equivalently the gain spectra $g(\omega)$=-$\alpha(\omega)$ are evaluated within the context of a Keldysh Nonequilibrium Green's function (NGF) approach. The susceptibility $\chi(\omega)$ is directly related to the carriers Green's functions G, which satisfies a Dyson equation,

$$\alpha(\omega) = \frac{4\pi\omega}{cn_b}\mathrm{Im}\{\chi(\omega)\}, \;\; \chi(\omega) = 2\sum_{\mu\neq\nu,\vec{k}} \wp_{\mu\nu}\, \chi_{\nu,\mu}(k,\omega). \tag{1}$$

Here n_b denotes the background refractive index, c is the speed of light, $\wp_{\nu\mu}$=$ed_{\nu\mu}$ is the transition dipole moment between the subbands ν and μ, which are labelled as "-", if belong to the lowest conduction band branch and "+", if belong to top CB branch (see Fig 1(a)). Thus in the discussion that follows, if electrons are injected in the subband e_{2+} and make a transition to subband e_{3-} creating a photon, this will be called a e_{2+} to e_{3-} transition. The numerical scheme used here can be summarised as follows: The first step is the solution of the 10 band $\mathbf{k}\cdot\mathbf{p}$ Hamiltonian which includes the dilute nitrogen levels responsible for the extra nonparabolicity that gives rise to strong differences in effective subband masses. The Green's functions and self-energies are expanded using eigenstates and eigenvalues of this Hamiltonian. The model system actually investigated in this paper is globally out of equilibrium but the electrons are assumed to be thermalised within each subband. For a feasibility study we control the total number of electrons in each subband, which can in practice be achieved, e.g. by optical pumping, selective doping or a combination of

3

both methods. Thus, the full NGF scheme is simplified and reduces to the self-consistent evaluation of chemical potentials and self-energy matrix elements which lead to subband energy renormalisation, dephasing constants and occupation functions. Finally, absorption and gain are given by the solution of the integro-differential equation for $\chi_{\nu\mu}(k,\omega)$ obtained from the carriers Green's function in linear response [9, 22, 23] The dephasing used in the numerical inversion is a frequency and momentum dependence approximation to the single-plasmon-pole dynamically screened dephasing of Ref 16 further simplified by a quasi-particle approximation with thermal distributions. The proof of concept structure chosen is a 7 nm $Ga_{0.98}N_{0.02}As/Al_{0.3}Ga_{0.7}As$ QW. From the lowest to the upper subband, the effective
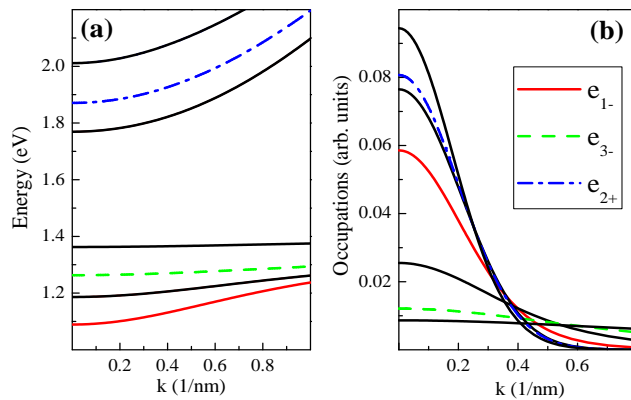

FIG. 1: (Colour online) Band structure and corresponding occupation functions (inset) assuming that all subbands have an electronic density of $n = 1.0 \times 10^{11} cm^{-2}$ thermalised at 300 K. The convention is the same in both panels.The solid, dashed and dot-dashed are, respectively for the subbands 1, 3 and 6 or equivalently e_{1-}, e_{3-} and e_{2+}. Local inversion in k-space is clearly seen.

masses (at **k**=0, are given by m_{1-}=0.125, m_{2-}=0.277, m_{3-}=0.820, m_{4-}=2.119, m_{1+}=0.118, m_{2+}=0.109 and m_{3+}=0.088. Those values are in good agreement with experiments [24]. Note that the energies are so nonparabolic that the concept of effective mass does not make sense in the whole Brillouin zone, but those values are useful to compare the curvatures in the most relevant region of k-space, i.e. around k=0.

The nitrogen level has been positioned to create upper bands (e_{1+} - e_{3+}) with lower masses that the lower states (e_{1-} - e_{4-}). Figure 2 shows the clear connection between larger N-content and larger masses in e_{3-} compared with e_{2+}. This leads to local inversion in k-space as shown in Fig. 1.b. Figure 3 further illustrates the existence of strong gain without
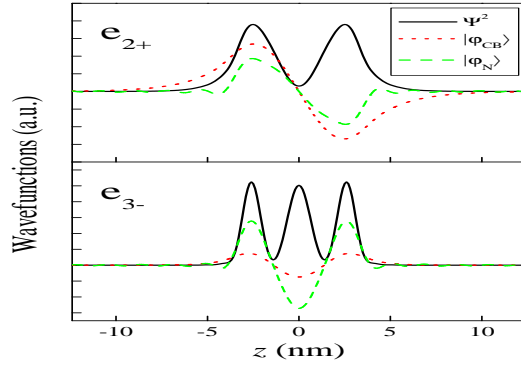
FIG. 2: (Colour online) Conduction-band character $|\phi_{CB}\rangle$ (dots), nitrogen-character $|\phi_N\rangle$ (dashed) and charge density Ψ^2 (solid) for e_{2+} (top) and e_{3-} (bottom).

inversion assuming bands e_{1-}, e_{3-} and e_{2+} only are occupied. In all panels the electrons are thermalised at 300 K. The allowed dipole moments ($\wp_{\mu\nu} = e d_{\mu\nu}$) are given by $d_{e_{1-},e_{2+}}$=0.216 nm, and $d_{e_{3-},e_{2+}}$=0.313 nm. The combination of larger dipole moment and specially larger differences in effective masses make the second transition the dominant. This large difference in effective masses allows for gain even if there is considerably more global occupation in the lower subband.

Note that cross absorption in the high energy side of the stronger transition compensates the small gain without inversion for the weaker transition. Furthermore it is interesting to notice that the dispersive gain expected for LWI [6, 25] is found for similar effective masses. See Fig. 3.b for the e_{2+} to e_{1-} transition, in which the upper and lower subband masses are given respectively by m=0.125 and 0.109. The dashed curve with equal densities in both subbands is the reference. In contrast, see the difference between the gain (around 600 meV) and the absorption regions (around 800 meV) in Fig. 3.c for the e_{2+} to e_{3-} transition in which the lower and upper masses are given respectively by m_{3-}=0.820 and m_{2+}=0.109. The dispersive shape is strongly distorted. Again the dashed curve with the same global density of carriers in both subbands is the reference.

It should be pointed out that typical intersubband relaxation times are generally short and that means that the pumping rate of the upper subbands should be large. Furthermore, the pumping mechanisms (carrier injection) do not populate the subbands homegeneously in general. Hence, at a very short time scale the populations around k=0 may be different
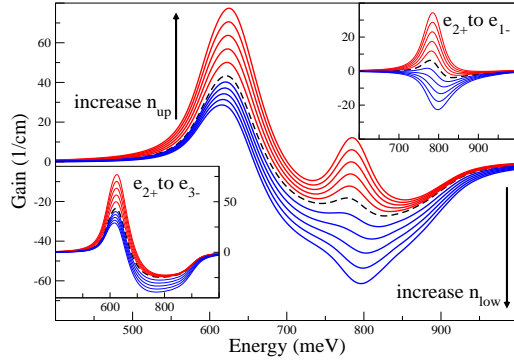
FIG. 3: (Colour online) Gain without global population inversion. In the dashed (black) curve, the density for the e_{2+}, e_{1-} and e_{3-} subbands is the same, $n_{up} = n_{low} = 1.0 \times 10^{11} cm^{-2}$. The (blue) curves below it have a fixed density in the e_{2+} subband $n_{up} = 1.0 \times 10^{11} cm^{-2}$ and from top to bottom, the (equal) density of subbands e_{1-} and e_{3-} increase by n_{low}=1.1, 1.2, 1.3, 1.4 $\times 10^{11}$. The (red) curves above the dashed line do not have global lasing without inversion and are here for a comparison. For those the (equal) e_{1-} and e_{3-} densities are fixed at $n_{low} = 1.0 \times 10^{11} cm^{-2}$ and from bottom to top the density of the e_{2+} subband increases by $n_{up} = 1.1, 1.2, 1.3, 1.4 \times 10^{11}$. The same convention for curves holds for the insets.

from the thermalized distributions used here. Note however, that we have given the first step towards addressing those issues by considering more global carriers in the lower subbands and (not shown) by approximating strongly nonthermal distributions by a limiting worst case in which the upper subband have electrons thermalized at higher temperatures. We still found considerable gain for the same global densities and electronic temperatures 100 K higher in the upper subbands. Future work will use an extended version of our fully nonequilibrium approach [16, 23] that will start from the solutions of the Hamiltonian used here for each layer. In summary, this theoretical proof of concept shows that it is possible to engineer conduction subbands with substantial differences in effective masses which make gain without global inversion feasible in dilute nitride heterostructures. We find a strong link between the similarity of effective subband masses and dispersive gain features with contrasting results for very different masses. Our study suggests that designs based on the dilute nitride band engineering approach proposed here, with suitably smaller energy differences between the subbands leading to gain in the THz range and including the required

depopulation channel, can deliver THz lasing at higher temperatures.

----

[1] J. Faist, F. Capasso, D.L. Sivco, C. Sirtori, A.L. Hutchinson, A.Y. Cho, Science 264, 553 (1994).

[2] N. Bandyopahyay, Y. Bai, B. Godken, A. Myzaferi, S. Tsao, S. Slivken and M.Razegui,Appl. Phys. Lett. **97**, 131117 (2010).

[3] S. Kumar, Q. Hu and J. Reno, Appl. Phys. Lett. **94**, 131105 (2009).

[4] B. S. Williams, Nat. Photonics **1**, 517 (2007).

[5] J. Faist, F. Capasso, C. Sirtori, D.L. Sivco, A.L. Hutchinson, M. S. Hybertsen and A. Y. Cho, Phys. Rev. Lett. 76, 411 (1996).

[6] A. Wacker, Nat. Phys. 3, 298 (2007).

[7] R. Terazzi, T. Gresch, M. Giovanni, N. Hoyler, F. Faist and N. Sekine, Nat. Phys. 3, 329 (2007).

[8] G. Sun, A. Liu and J.B. Khurgin, Appl. Phys. Lett. **72** 1481 (1998).

[9] M.F. Pereira Jr., Phys. Rev. **B 78**, 245305 (2008)

[10] W. Shan, W. Walukiewicz, and J. W. Ager, III, E. E. Haller, J. F. Geisz, D. J. Friedman, J. M. Olson, and S. R. Kurtz, Phys. Rev. Lett., **82**, 1221 (1999).

[11] P. J. Klar et al, Solid State Electron. **47**, 437 (2003).

[12] S. Tomić, E.P. O'Reilly, P.J. Klar, H. Gruning, W. Heimbrodt, W.M. Chen and I.A. Buyanova, Phys. Rev. B **69**, 245305 (2004).

[13] Y.X. Dang and W.J. Fan, Phys. Rev. **B 77**, 125334 (2008).

[14] J.-Y. Duboz, Phys. Rev. **B 75**, 045327 (2007).

[15] J.-Y. Duboz, J. A. Gupta, M. Byloss, G. C. Aers, H. C. Liu, and Z. R. Wasilewski, Appl. Phys. Lett. **81** 1836 (2002).

[16] T. Schmielau and M.F.Pereira Jr, Appl. Phys. Lett. **95** 231111 (2009).

[17] S. Tomić, E. P. O'Reilly, R. Fehse, S. J. Sweeney, A. R. Adams, A. D. Andreev, S. A. Choulis, T. J. C. Hosea, and H. Riechert, IEEE J. Select. Topics Quantum Electron. **9**, 1228 (2003).

[18] A. Patane, J. Endicott, J. Ibanez, P. N. Brunkov, L. Eaves, S. B. Healy, A. Lindsay, E. P. O'Reilly, and M. Hopkinson, Phys. Rev. B **71**, 195307 (2005).

[19] L. Ivanova et al, Phys. Rev. B **82**, 161201(R) (2010).

[20] A. Lindsay and E. P. O'Reilly, Phys. Rev. Lett. **93**, 196402 (2004)

[21] I. Vurgaftman, J. R. Meyer, and L. R. Ram-Mohan, J. Appl. Phys. **89**, 5815 (2001).

[22] M.F. Pereira Jr. and H. Wenzel, Phys. Rev. B70, 205331 (2004).

[23] M.F. Pereira Jr., S.-C. Lee and A. Wacker, Phys. Rev. B69, 205310 (2004).

[24] P.N. Hai, W. M. Chen, I. A. Buyanova, H. P. Xin, and C. W. Tu, Appl. Phys. Lett **77**, 1843 (2000)

[25] D.G. Revin, M.R. Soulby, J.W. Cockburn, Q. Yang, C. Manz and J. Wagner, Appl. Phys. Lett. **92** 081110 (2008)